In: AIAA SciTech Forum 2023, National Harbor, 23-27 January 2023, Maryland, USA
DOI:10.2514/6.2023-2133

The Impact of Electric Machine and Propeller Coupling Design on Electrified Aircraft Noise and Performance

A. Kiran* and B. Zaghari†
School of Aerospace, Transport and Manufacturing, Cranfield University, MK43 0AL, UK

T. Sinnige‡
Delft University of Technology, Kluyverweg 1, 2629 HS Delft, Netherlands

E. Pontika§ , H. Balaghi Enalou¶ , T. Kipouros‖ and P. Laskaridis**
School of Aerospace, Transport and Manufacturing, Cranfield University, MK43 0AL, UK

Novel propulsion systems have been studied in literature to reduce aircraft emissions with hydrogen or other electrical energy sources. Hybrid Electric Propulsion (HEP) system consists of electric machines as an alternative way to provide power for propulsion resulting in the reduction of aircraft fuel consumption. While reduction of emission is the main driver of new HEP designs, aircraft noise reduction and performance improvement will also need to be investigated. Much quieter electrified aircraft than conventional aircraft is explored with considering the benefits of coupled design between the propeller and electric machines. In this study, several electric machine designs have been explored and coupled with the propeller design to study the trade-off between the aerodynamic and acoustic performance of the propeller. Aerodynamic optimization is used as a baseline to minimize the energy consumption to find the aerodynamics optimum subject to constraints on the thrust levels during the mission. The propeller aerodynamic optimizer considers the electric machine efficiency map, which is a function of propeller torque and rotational speed, to find the optimum combination of propeller and electric machine designs. The objective function of the acoustic optimizations is to reduce the cumulative noise level over the entire mission. It is shown that a wider envelope of peak motor efficiency in the efficiency map provides acoustics and aerodynamic performance benefits. The trade-offs between reducing noise or increasing aerodynamic efficiency to reduce energy consumption are demonstrated.

I. Nomenclature

C_P	=	Coefficient of Power
C_T	=	Coefficient of Thrust
J	=	Advance ratio
T_C	=	Thrust Coefficient
h	=	Altitude in meters
V_∞	=	Free stream velocity
t	=	Time duration in minutes
E	=	Energy consumption
p_{rms}	=	Acoustic pressure oscillation
D	=	Diameter of the propeller
T	=	Thrust

*PhD Candidate, Centre for Propulsion and Thermal Power Engineering, abhishek.kiran@cranfield.ac.uk
†Lecturer, Centre for Propulsion and Thermal Power Engineering, bahareh.zaghari@cranfield.ac.uk, AIAA member
‡Assistant Professor, Flow Physics and Technology Department, t.sinnige@tudelft.nl, AIAA member
§Research Fellow, Centre for Propulsion and Thermal Power Engineering, evangelia.pontika@cranfield.ac.uk, AIAA member
¶Research Fellow, Centre for Propulsion and Thermal Power Engineering, hb.enalou@cranfield.ac.uk
‖Senior Lecturer, Centre for Propulsion and Thermal Power Engineering, t.kipouros@cranfield.ac.uk, AIAA member
**Professor, Centre for Propulsion and Thermal Power Engineering, p.laskaridis@cranfield.ac.uk, AIAA member

Published by AIAA. This is the Author Accepted Manuscript issued with: Creative Commons Attribution Non-Commercial License (CC:BY:NC 4.0).
The final published version (version of record) is available online at DOI:10.2514/6.2023-2133. Please refer to any applicable publisher terms of use.

$TSSP$ = Thrust-Scaled Sound Pressure level

II. Introduction

The need for more sustainable aviation and the increasing demand for short-range passenger transportation has led to a renewed interest in propellers by the research community. Propellers can provide aircraft propulsion with exceptionally high aerodynamic efficiency. However, as opposed to the high aerodynamic efficiency of the propeller, the acoustic performance of the propeller is not as favorable. Therefore, to make propellers more attractive for application on future aircraft, their noise emissions need to be minimized by improving blade design and propeller operating conditions while maintaining high aerodynamic efficiency. For most hybrid electric aircraft, the propeller is driven by a motor, which should be designed to support the propeller design, to achieve minimal noise emissions. To this end, co-designing the propeller and the electric machine becomes crucial.

In the current literature matching the propeller and the electric machine is considered to improve the overall efficiency and propulsion performance, while reducing the total weight. Matching in the present context is defined as finding the point or region where the motor and the propeller can both operate at higher efficiencies and achieve the mission performance objectives such as reducing noise, carbon, and non-carbon emissions, lowering weight, and reducing fuel consumption. The integration of the propeller and the motor is critical in identifying the operating and design points for the electric machine and the propeller, to ascertain the total efficiency of the integration while maintaining lower noise. For the matching, the propeller model, electric machine model, and mission performance are required to be assessed integrally.

The studies presented in [1–4] describe matching using three criteria, using propeller performance curves, an electric motor efficiency map, and flight conditions. The propeller model was used to obtain various parameters such as Coefficient of Thrust (CT), Advance Ratio (J), Coefficient of Power (CP) Torque, and RPM for these studies. McDonald. R in [2] chose the flight condition as an equilibrium flight. McDonald. R in [2] stated that due to the popularity of the constant speed propeller, an alternate form of the propeller thrust coefficient CT was devised to achieve an optimum pitch scheduling for propeller-airframe matching. Furthermore, the performance of various types of propellers was shown and their impact on aircraft performance was discussed but the source of the shaft power supplied to the propeller was not considered for this study. McDonald. R also used this approach in [1], where a similar method was adopted to match a ducted fan to an electric motor.

In [3], the problem was addressed by drawing the contour of the three parameters: motor efficiency, propeller efficiency, and flight condition, which in this study was considered, flight speed and climb rate. The possibility of three different flight speeds was also investigated to analyze flight conditions that would better fit in the matched region. Furthermore, in [5] an iterative process was used to match the propeller and motor, the process involves using the rotational speed in RPM to find the power of the propeller and the power of the motor from the respective models. The difference between these two values was calculated and if the error is below a predefined value, then the motor and propeller were matched. However, in these studies, [3][5] the design of the propeller and the motor are done separately.

In literature involved with the matching of propeller and electric motor, the flight conditions considered are either equilibrium flight or climb rate. The hypothesis is that for various flight phases the thrust demands, propeller pitch, and the motor operating point would be different, and to identify an efficient system these need to be taken into consideration. For an in-depth analysis of the propeller motor matching, each flight phase for a given mission should be taken into consideration for a particular configuration of the electric motor and propeller. In this study, when the motor and propeller are coupled, every flight phase is taken into consideration to find efficiencies for the motor and propeller.

To better communicate to trace requirements and establish a relationship for decision-making in matching electric engine and propeller, a System Engineering (SE) approach has been adopted [6]. This paper explains the propeller design, motor design, and the approach taken to match their interactions to achieve lower noise emission while having higher performance and higher efficiency. The emphasis of this paper is to provide the reader with an understanding of the integration efforts and the various trade-off studies that may be made based on the needs of the mission.

Optimizing a fan and motor together yields different results than using a motor-only design. In [7], the co-design of the motor and propeller are investigated in an optimization framework with the key objectives of overall efficiency and reducing the mass of the system. The study concludes that a smaller propeller count is more suitable for both efficiency and mass considerations. In [8], a similar optimization framework is utilized using a Superconducting motor. A 32-motor configuration is shown as optimum but due to the complexity in the design and integration of these motors, a 9-motor configuration is finally concluded as the optimum using 2.4 MW motors which would be used in direct drive applications along with a fan. In [1–3], a parametric model of the motor was considered for the matching process, while

these models are very useful for the conceptual design stage however when progressing higher level of the design phase a more detailed motor model is required to calculate the efficiency and feasibility of the motor to support propeller design requirements.

Most electric machines have higher specific power at a higher rotational speed. However, to match the electric machine with the propeller directly, lower rotational values (<4000 RPM) need to be considered. Designing a machine at a lower RPM affects its weight, size, and efficiency. The efficiency of electrical machines for a given torque and rotational speed is shown as an efficiency map. This map can be obtained using analytical approaches using machine fundamental equations [9] using a d-q model [10] and high-fidelity finite element models [11] and a genetic algorithm [12]. Machine fundamental equations allow fast integration of the machine into the rest of the system, however, does not scale well when system parameters need to be explored for a wide range of studies. Hence, the machine characteristics based on the fundamental equations should be used cautiously. The design process and simulations also depend on the type of electric machines. Currently, for most of the electrified propulsion, the effort has been on exploring Permanent Magnet Synchronous Machines (PMSM). A study conducted by Samith in [13], showed the comparison of various motors that are available and assessed eight different types of motor topologies, the study concluded that PMSM and BLDC are better candidates for aerospace applications due to their specific power, compared to other topologies investigated. Xie in [11] proposed a sizing procedure for Surface Mounted Permanent Magnet Machines (SMPMM), the procedure is for either the outer rotor or inner rotor machine. Existing analytical methods were compared with a high-fidelity finite element method and a small error was reported. However, this method is not scalable [11], and the design exploration needs to be repeated if the requirement changes. A study was conducted in [14] to identify the optimal voltage and current selection for a turbo-electric propulsion architecture. A design approach based on torque capabilities (Torque per volume, TRV) and flux propagation was presented. The effect of the DC voltage selected for the machine inverter on the weight and efficiency of the machine was explored. Since the machine design parameters have not been revised for each DC voltage selection, the efficiency and the specific power of the machine are only valid for small variations of machine parameters.

The paper is divided into various sections, Section III.A explains the flight mission and phase and the medium that was used to explore the design space. Section IV explains propeller design methodology and optimization work, and Section V explains the motor design methodology and modeling efforts. Results for the integration of the propeller and electrical machine are presented in Section VI.

III. Selected Electric Aircraft Propulsion

A fully electric Fuel Cell (FC) propulsion system is retrofitted to a 4MW, 70-passenger turboprop regional aircraft. Public data available for the ATR72 are used to model the baseline aircraft [15].

The aircraft performance and mission analysis, the electrical architecture, and the motor design are provided using CHARM methods and tools. CHARM is the Cranfield Hybrid electric Aircraft Research Model which is an integrated approach to explore various electrified propulsion technologies and their synergies. It comprises methods and tools for modeling and evaluating conventional and novel aircraft configurations [16][17][18], designing and analyzing the performance of electric components, electrified architectures (E-HEART) [19][20] and thermal management systems, and integrating them with the aircraft performance and mission analysis. The flight mission analysis is performed using Hermes, the in-house aircraft performance platform at Cranfield University [16] for a fully electrified aircraft with a propulsion architecture shown in Fig. 1.

The electrical architecture is modelled and analyzed using the Cranfield in-House E-HEART (Enabling-Hybrid Electric Aircraft Research and Technology) tool which is part of CHARM. This modeling tool integrates all the electrical components and analyses their interactions at component and their integration levels. Different modeling approaches, from low-fidelity fundamental equations to high-fidelity models, such as finite element analysis for electric machines, and dynamic modeling of power electronics are included in E-HEART. E-HEART is part of a digital-twin model being developed. The low fidelity FC model in E-HEART has been explained in [21] and [22].

A. Mission Requirements

In the retrofit approach, the same Maximum Take-Off Weight (MTOW) and fuselage volume must be maintained, since the aircraft lifting surfaces are not re-designed. Consequently, the flight mission analysis in this optimization study is performed for the MTOW of a conventional aircraft. Figure 2 shows the altitude, velocity, net thrust (propeller thrust), and total power from the mission analysis.

When the optimized propeller-motor system is integrated back into the mission, the trade-off between the available

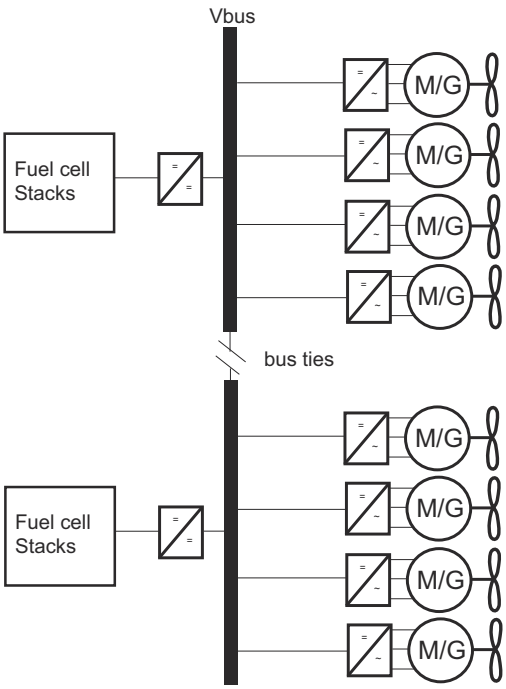

Fig. 1 Full electric propulsion system consists of eight motors and propellers.

mass for payload and the Operating Empty Weight (OEW) changes based on the new propeller and motor masses, while the MTOW constraint is maintained. Other mission specifications, climb speed, ambient conditions, cruise altitude, and cruise Mach are included in Table 1.

Table 1 Mission parameters

Parameter	Value
Take-off Weight (MTOW)	23000 kg
Operating Empty Weight (FC Retrofit)	15936 kg
Range	300 nmi
Payload	6722 kg
Fuel Capacity	450 kg
ISA Temperature Deviation	0 K
Calibrated Climb Speed	170 knots
Cruise Altitude	17000 ft
Cruise Mach	0.44

The selection of eight propeller propulsion architecture is based on the trade-off between the torque demand at a given propeller rotational speed and the motor torque density. For a two-propeller configuration, the rotational speed of the propeller is higher compared to the eight-propeller configurations. This leads to an increase in torque demand for a two-propeller configuration in comparison to the eight-propeller configuration while the required propulsion power is the same in both cases. The torque demand during take off, climb, cruise, and descend for different propeller configurations are calculated and shown in Fig. 3. The required torque for each propeller is higher when a lower number of propellers are considered due to a decrease in rotational speed for a fixed aircraft power requirement. Designing electrical machines to provide higher torque, which are heavier machines, is challenging, and hence in this study, an eight-propeller architecture is selected as shown in Fig. 1.

The first estimate of the flight mission analysis is performed using generic, non-optimized propeller and motor

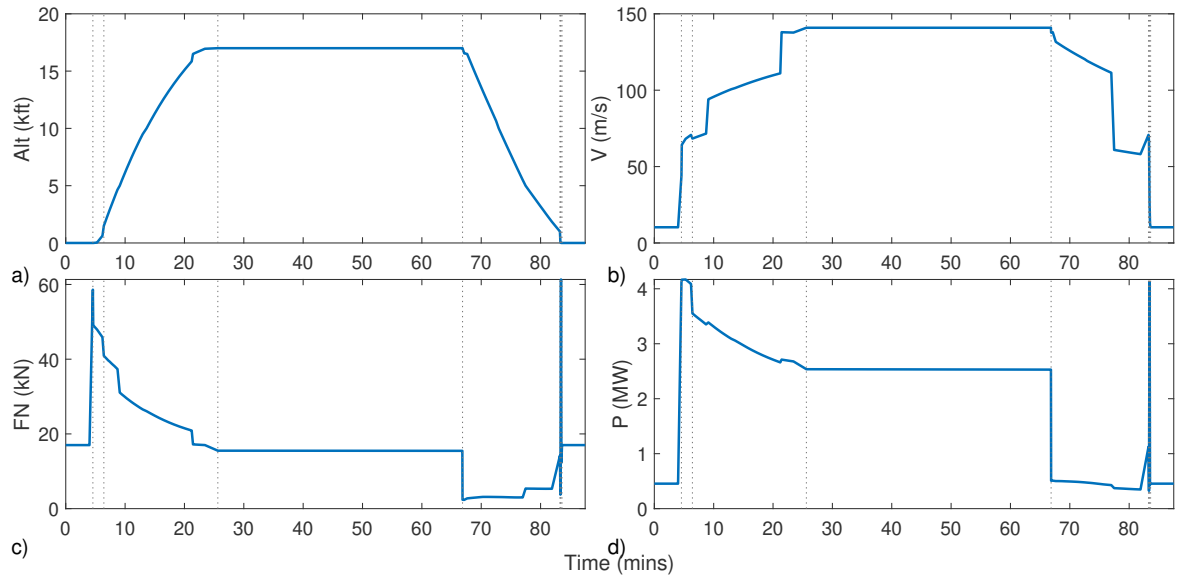

Fig. 2 (a) Altitude, (b) Velocity, (c) Net thrust, and (d) Total power from the mission analysis.

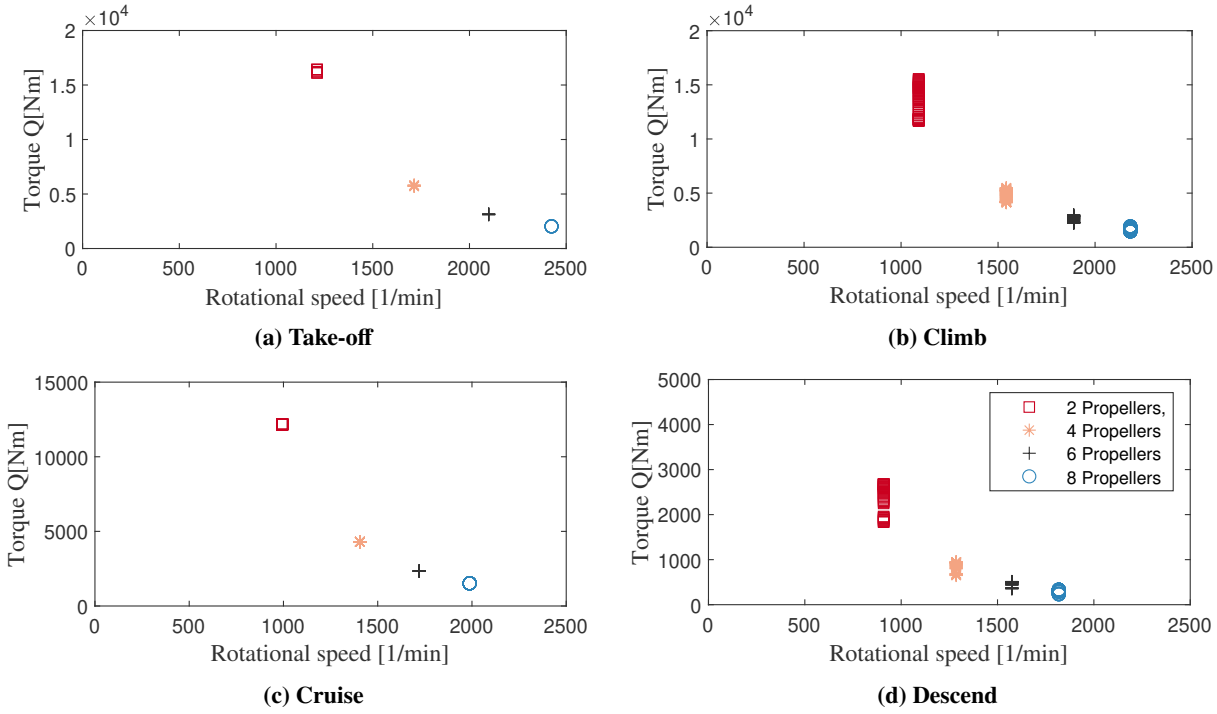

(a) Take-off **(b) Climb**

(c) Cruise **(d) Descend**

Fig. 3 Required torque to rotate each propeller at the rotational speed defined for each mission phase according to baseline mission analysis. Four configurations, with two, four, six, and eight propellers are shown.

models. The propeller model map communicates with the flight mission analysis through the advance ratio, which is a function of aircraft velocity and rpm, and the altitude to obtain the air density. The propeller model also interfaces with the electric motor by receiving as input the output shaft power of the motor. The initial flight mission analysis provides inputs to propeller optimization and motor matching. Each combination of shaft power and the advance ratio has a unique point on the $Cp - J$ propeller map for a given air density (altitude) which corresponds to a unique pitch angle. Then, the thrust produced by the propeller can be calculated by referring to the advance ratio and pitch angle of this

operating point. The produced thrust is returned to the aircraft performance model for the calculation of the acting forces on the aircraft and acceleration/deceleration. At the same time, the consumed fuel by the FC system is removed from the aircraft's weight.

After the propeller and motor have been matched and optimized for mass, aero-acoustics, and efficiency, based on the given flight path, the mission can be re-iterated using the new propeller and motor maps as well as new masses which will alter the available weight allowance for payload (also shown in Fig. 4). The re-iterated mission is expected to deviate from the initial mission in three ways:

1) The efficiency of the system will have changed so the energy/fuel consumption will be different.
2) The new weight difference between MTOW and OEW plus fuel will be allocated for the payload.
3) The optimized propeller diameter changes depending on the rpm range (so that the tip Mach Number does not reach transonic speeds) which will influence the drag characteristics of the aircraft which in turn will impose a different thrust required to maintain the same aircraft performance (ex. climb time, cruise at same Mach & altitude).

Figure 4 presents the workflow and the interconnectivity between the mission, propeller, and electric machine modeling. This diagram shows the parameters and analysis that are considered in our coupled design.

The motor is designed for various levels of torque and length, these designs are then passed on to the propeller optimization segment. The propeller designs are optimized with the motor design as explained in section IV. The propeller optimization results and the trade-off analysis is explained in section VI. After the trade-off analysis, the thermal management of the motor is rechecked based on the new operating that are the result of the propeller optimization, as seen in section V.B.

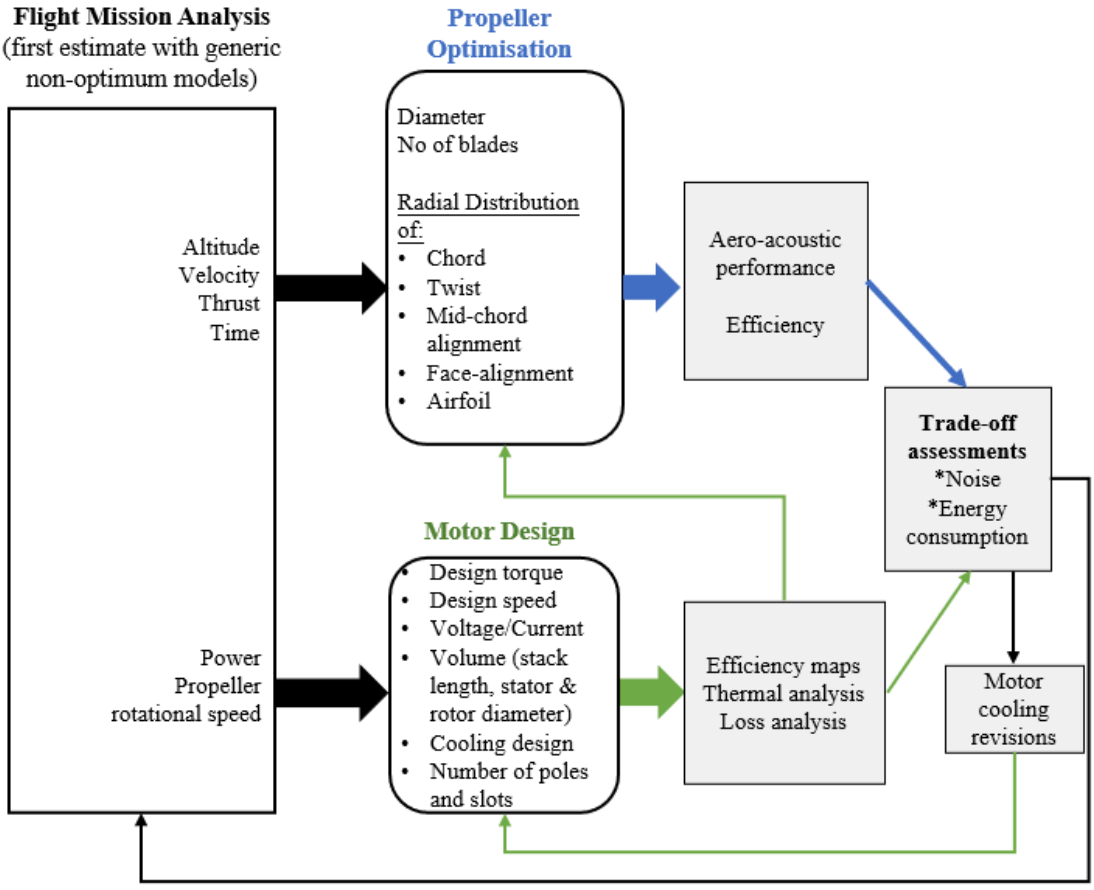

Fig. 4 Co-design parametric study of propeller and electric machine for a given mission of a fully electrified fuel cell aircraft.

IV. Propeller Design Methodology

In this study, the propeller design is optimized for several different motor designs. In a real configuration, the interaction between the airframe and the propeller leads to an unsteady blade load due to non-uniform inflow. This impacts the propeller efficiency, noise emissions, and vibrations. For this study, however, the propeller is considered in isolation to limit complexity.

The propeller geometry was defined by the following parameters:

- Diameter: D
- Number of blades: N_B
- Radial chord distribution: $c(r)$
- Radial twist distribution: $\theta(r)$
- Radial mid-chord-alignment distribution: $MCA(r)$
- Radial face-alignment distribution: $FA(r)$
- Radial airfoil distribution

To limit the number of variables and the scope of the paper, the following assumptions were made:

- The diameter was fixed at $D = 1.96$ m;
- The number of blades was fixed to $N_B = 6$;
- Blade sweep and face alignment were not considered for this study and were set to 0;
- The blade airfoils were not modified with respect to the baseline propeller (TUD-XPROP, see [23, 24]).

The radial distributions of chord and twist were parameterized using third-order Bézier curves. The radial position of the first and last control points was fixed to the hub and tip, respectively. The twist at the tip was defined as zero for the optimization, with the collective pitch angle defined there. For the presentation of the results, the twist distribution was shifted to have the reference collective pitch angle defined at $r/R = 0.7$. With these choices, 11 design variables were required to describe the blade planform shape.

The nature of the mission profile for hybrid-electric aircraft implies that considering a single cruise design point is not sufficient for optimization purposes, as most aircraft do not spend a dominant part of the mission time and energy in the cruise segment. Choosing a single design point might make the system inefficient in other segments where the aircraft would spend more energy, such as climb. So, the whole mission is considered in the propeller design phase. It was decided to split the mission into 5 segments: take-off (TO), initial climb (CL1), top of the climb (CL2), cruise (CR), and descent (DS). To limit the number of function calls and design variables, for each of these mission segments the conditions were assumed constant for the duration of the mission segment. Table 2 defines the operational conditions considered for each of the mission segments.

Table 2 Definition of mission segments for propeller-motor optimization.

Mission segment	h [m]	V_∞ [m/s]	$T_C = \frac{T}{\rho_\infty V_\infty^2 D^2}$	t [min]
Take-off (TO)	0	60	0.400	2.0
Initial climb (CL1)	1000	70	0.230	2.5
Top of climb (CL2)	3650	100	0.090	15.0
Cruise (CR)	5200	140	0.035	43.0
Descent (DS)	3000	120	0.020	15.0

For each of the mission segments, the propeller advance ratio and pitch setting are optimized, adding 10 design variables next to the 11 planform design variables. Bounds were defined on all design variables to avoid unfeasible blade shapes and operating conditions.

The aerodynamic and acoustic performance of the propeller was evaluated using a blade-element momentum method coupled to a frequency-domain acoustic solver that implements Hanson's method. More details are provided in [25]. Optimizations were then performed with a gradient-based method (SQP), using finite differences to estimate the gradients.

Different objective functions were used. Baseline optimizations were performed with an objective function focused on aerodynamic performance. To describe the performance over the entire mission, the objective for the optimization was based on the sum of the energy consumption E (based on shaft power P) during each of the considered mission

segments:

$$E = \sum_{i=1}^{N} E_i = \sum_{i=1}^{N} P_i t_i, \tag{1}$$

where i refers to the segment in the mission profile, N to the number of segments in the mission profile considered ($N = 5$), and t to the time of each segment. The combined efficiency of the propeller and motor was considered in the optimization. Any other losses in the power train (transmission, etc.) are not accounted for. The propeller efficiency was obtained directly from the blade-element-momentum solution, while the motor efficiency was obtained from interpolation in the computed motor efficiency maps. Equality constraints were used to ensure that the prescribed thrust is delivered by the propeller. Inequality constraints were defined to limit the total shaft power.

Following the aerodynamic optimizations, acoustic optimizations were performed with an objective function focused on the propeller noise emissions. These were defined in terms of the thrust-scaled sound pressure level (TSSP)

$$TSSP = 20log_{10}\frac{p_{\text{rms}}D^2}{T}, \tag{2}$$

where p_{rms} is the rms value of the acoustic pressure oscillation. The objective function of the acoustic optimizations was to reduce the cumulative noise level over the entire mission. For each mission segment, noise levels were computed for axial directivity angles ranging from 30 to 150 deg, in steps of 15 deg, at a radial distance of 5 times the propeller radius. These levels were then summed (logarithmically) to obtain the final noise metric. For the selected operating conditions, the take-off and initial climb segments dominated the cumulative noise level.

The constraints used for the aerodynamic optimization are also applied for the acoustic optimization. An inequality constraint was added to limit the energy penalty with respect to the performance obtained with the aerodynamic optimum. Penalty levels of 0.5%, 1.0%, 2.0%, and 5.0% were considered to study the trade-off between aerodynamic and acoustic performance.

V. Electric Machine Selection and Design

The design methodology for electric machines is proposed not only based on the requirements set by the mission and propeller but also on the machine's optimum performance. A heuristic approach for modeling PM machines for use in aircraft propulsion has been adopted in this study. Based on the baseline mission data, the maximum torque and rotational speed of each propeller are calculated. The maximum torque corresponds to the torque during take-off ($T_{\text{take-off}}$). The torque and the rotational speed at take-off can be considered the design parameter for the electric machine. Higher ratios of torque are considered in this study to provide higher efficiency at a given operational point. Hence, a factor of 1.4, 1.6, 1.8, and 2 is multiplied by the take-off torque to show four designs at higher design torque values. The electric machine rotational speed is designed for the propeller rotational speed at take-off. In this study, four different designs are considered (shown in Table 3). These four designs are defined based on the mission requirements and the variation in rotational speed and torque required for several case studies of propeller aerodynamic and acoustic optimization. In this study, an Interior Permanent Magnet Machine is considered (Fig. 6). Machine fundamental equations are used after identifying the electric machine design parameters such as speed, torque, DC-Bus voltage, volume, and the cooling method, to define the detailed FEM electric machine model in ANSYS Motor-CAD (Fig. 6). The machine is defined for today's technological considerations.

Table 3 Electric machine input design parameters for four designs.

Design	Speed (rpm)	Torque (N.m)	DC bus voltage (V)	Max stator current (A)	Stack length (m)
#1	2424	$T_{\text{take-off}}\times 1.4 = 2875$	1400	600	0.21
#2	2424	$T_{\text{take-off}}\times 1.6 = 3285$	1600	600	0.24
#3	2424	$T_{\text{take-off}}\times 1.8 = 3696$	1800	600	0.27
#4	2424	$T_{\text{take-off}}\times 2 = 4106$	2000	600	0.30

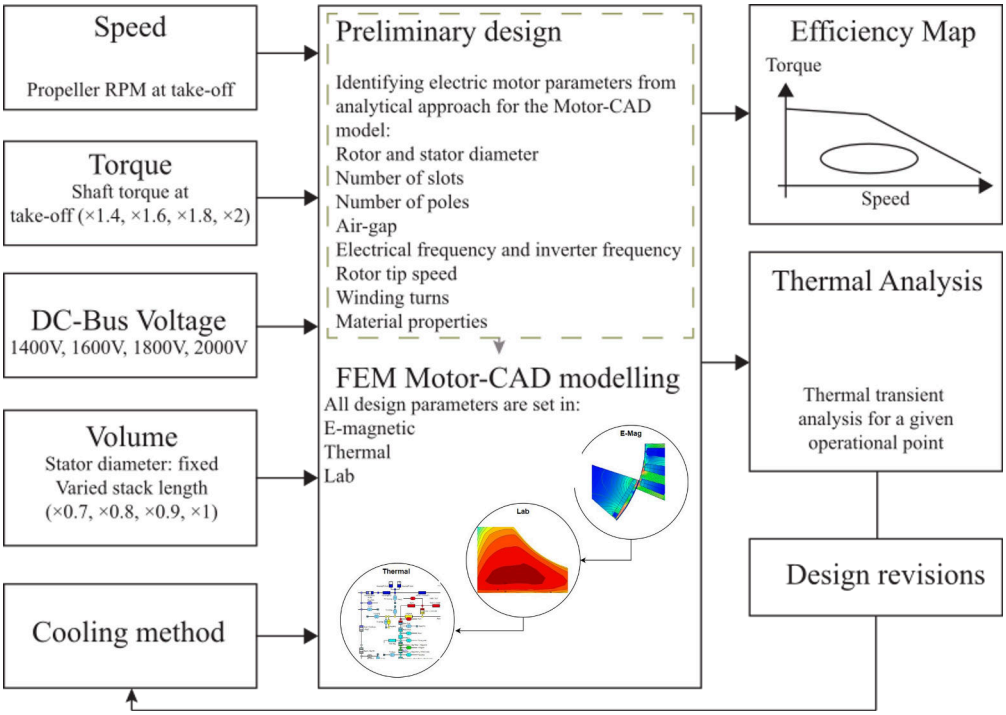

Fig. 5 IPM electric machine design process proposed for the requirement sets by the baseline mission and propeller optimization process.

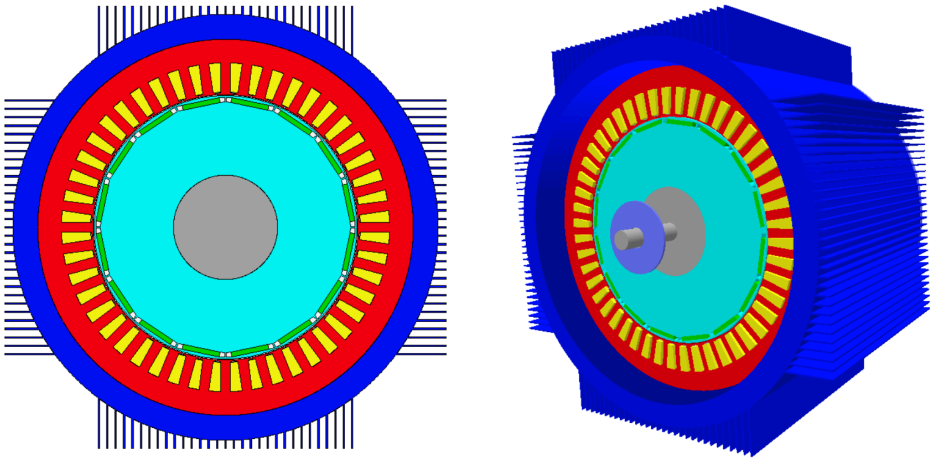

Fig. 6 Cross section and side view of IPM machine designed in ANSYS Motor-CAD.

A. Electric Machine Parameter

The design space for an electric machine to supply the torque needed is vast and so certain assumptions of the radial geometry have been made to focus the study more on the methodology of the integration. The electric machine volume, the stator diameter, and the stack length are chosen based on the boundaries defined by the propeller diameter and the required torque, respectively. The stack length is extended when higher torque requirements have been imposed. The stator diameter of the motor was set so as to not be more than 0.25 times the diameter of the propeller. A pole-slot combination was chosen [9] to ensure that the winding factor would be an integer to ensure a single layer winding for a 3-phase current and so a 16 pole 48 slot combination was chosen. The motor is designed with presently available technological considerations, no account for future variation is taken for this study. For all designs, the stator diameter is 0.450 m, the rotor diameter is 0.317 m, and the air gap is 0.00125m. The radial design parameters of the motor can be

seen in Table 4. The cooling method is defined as air-cooled, more about the thermal analysis is mentioned in Section V.B. These inputs to the electric machine design process are shown in the design process in Fig. 5.

Table 3 shows the input parameters selected for four designs. Parameters such as machine stator and rotor diameter, number of slots and poles, air gap, electric frequency, inverter switching frequency, rotor tip speed, and winding turns, including all material properties are defined in ANSYS Motor-CAD from the analytical model. Table 5 shows the output parameters obtained from the FEM analysis. Efficiency maps and thermal analysis were obtained from ANSYS Motor-CAD and the results are used to iterate the design process and revise the design. The output of this process is the efficiency maps, presenting the changes in torque, rpm, power, voltage, current, and motor efficiencies.

Table 4 Radial design parameter used for the motor

Machine Radial Parameter	Value	Machine Radial Parameter	Value
Slot Number	48	Pole Number	16
Stator Lamination Diameter (mm)	450	Slot Depth (mm)	38
Tooth Width (mm)	12	Slot Opening (mm)	1.5
Slot type	Parallel Tooth	Rotor type	Interior Flat (web)
Coil style	Stranded	Winding turn	10
Winding throw	3	Winding type	Lap
Divider type	Overlapping	Wire Gauge	AWG 17
Wire slot fill	0.494	Winding connection	Star Connection
Magnetization	Parallel	Magnet Thickness (mm)	6
Magnet Width (mm)	45	Airgap (mm)	1.25
Shaft Diameter (mm)	125	Electric Loading (Amps/m)	1.44

Table 5 Results obtained from ANSYS Motor-CAD for four designs.

Design Variables	#1	#2	#3	#4
Aspect ratio	2.14	1.88	1.67	1.5
Weight (kg)	241.7	282.2	316.7	348.3
Losses (kW)	41.51	47.86	52.99	57.47
Torque per rotor volume (kNm/m^3)	167	125.4	167.05	125.39
Speed limit for constant torque (RPM)	2208	2955	2237	3002.7
Maximum Torque (Nm)	2807	3537.3	3575	4421.5
Maximum Power (Kw)	586	672	772	862
Maximum Efficiency(%)	97.25	97.35	97	97.3
Continuous Power at maximum Efficiency (kW)	242	278	297	360

Torque and the rotational speed of the propeller are considered as the input parameters to explore the propeller and the machine's efficiencies. However, the impact of this matching on the HEP system cannot be explored with only a few parameters. Since the machine voltage and current, its envelope and weight, the cooling methodology, and its vibration and failure modes, affect the size and efficiency of the other sub-system components in the power distribution systems, a more detailed analysis of matching the electric machines and the propeller is required.

B. Thermal analysis

Forced air convection is preferred for motor cooling as opposed to liquid cooling due to the added complexity and weight of an extra thermal management system that is integrated with the aircraft. However, due to the compact design of motors striving for higher power density for aircraft applications, the air cooling system was not able to keep the machine within the acceptable temperature limits, since this is a low RPM - high Torque machine and this would not

allow forcing more air within the motor.

In literature, it can be observed that liquid cooling is implemented for the motor used for aerospace applications [26]. The cooling system of the motor should be designed to keep the winding and magnet temperatures within the acceptable limit, below 180°C. This is with the assumption that a NEMA (National Electrical Manufacturers Association) class H insulation is used [27]. The decision was made to use the slot water jacket option because it was observed the winding heated up quickly. The cooling system includes slot water jackets where the Water-Ethylene-Glycol (EGW) 60/40 cooling liquid flows in the space between the conductors to keep the winding temperature below 180°C. The required EGW mass flow is 1 liter/second with a maximum inlet temperature of 70°C which is a requirement for the thermal management system (TMS) of the aircraft. The ambient temperature for this study was set as 43°C, to simulate a hot day take-off operation.

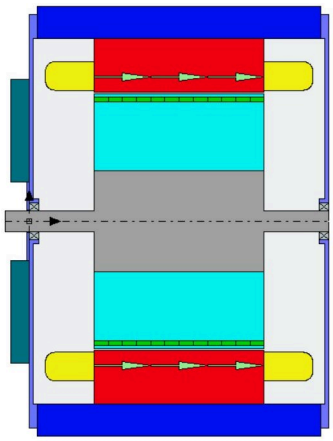

Fig. 7 Axial view of the motor; the green arrows indicate the proposed liquid cooling channel for the design

Thermal analysis is needed to ascertain the temperature of the motor during the operating points of the mission, mentioned in Fig. 10, to ensure the motor is viable. For each motor design, the thermal analysis has been explored in Motor-CAD, which uses a lumped thermal network model to calculate the temperature of the individual components of the motor.

Using these inputs and using a steady state analysis the maximum temperature reached by the winding is 126°C in motor design #1 and for motor design, #4 the temperature was 120°C. Steady-state analysis results for the aforementioned cases are within the thermal limits, this implies that the temperature constraint for various transient envelops is already met. When analyzing the motor performance for the whole mission and various other operational aspects. A transient analysis was also done for the mission segments defined in section III.A. The temperature within the winding and the magnet for motor design #1 reached a peak of 145°C and 113°C respectively and for motor design, #4 it was 158°C and 126°C respectively. For motor design #1, it can be observed that the long design of the motor, enables it to reach a lower temperature than compared to motor design #4 which is a smaller motor in terms of length.

VI. Propeller Optimization Results

With the 4 motor designs defined, the propeller optimization routine was performed. Propellers were designed for each motor design, both for the aerodynamic and acoustic objectives and constraints (i.e. 6 optimizations per motor). Figure 8 compares the aerodynamic and acoustic performance of each of the motor combinations. Each marker corresponds to an individual propeller design.

For a given motor design, Fig. 8 displays the expected trade-off between energy consumption and propeller noise. Quieter propeller designs come at the cost of increased energy consumption. However, clear differences in performance can be observed between the different motor designs. For given energy consumption, an increasing noise reduction is observed for increasing motor size (increasing motor design #). Comparing motor designs 1 and 4, the noise reduction is 2-5 dB, depending on the desired energy consumption level. Alternatively, an energy consumption benefit can be obtained for a given noise level. Again comparing the performance of the propeller-motor combinations for motor designs #1 and #4, a reduction in energy consumption of 0.5% to 2.5% is observed for the designs with motor design #4.

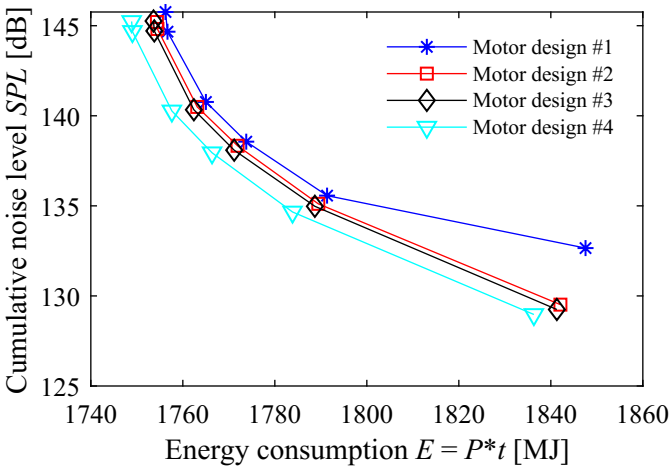

Fig. 8 Trade-off between energy consumption and propeller noise emissions for combined motor-propeller optimization. Lower energy consumption signifies higher high energy efficiency.

Both for energy consumption and noise, the largest performance benefit is obtained around the aerodynamic optimum, which is the most realistic design condition.

Analysis of the propeller and motor efficiencies shows that the largest performance benefit is obtained from the motor side. Figure 9 compares the propeller and motor efficiencies for the different motor-propeller combinations obtained from the aerodynamic optimization (i.e. objective to minimize combined energy consumption). It can be seen that the propeller efficiency for each mission segment is similar between the different motor-propeller combinations (Fig 9a), with a maximum difference between the cases of $\Delta\eta_p = 0.0005$. The motor efficiency (Fig. 9b) shows larger variations, with a maximum difference of $\Delta\eta_m = 0.015$ between motor designs #1 and #4 for the take-off condition, with better performance for the bigger motor (design #4). This suggests that the propeller designs obtained for the different motors were similar, which was confirmed by a comparison of the values of the design variables.

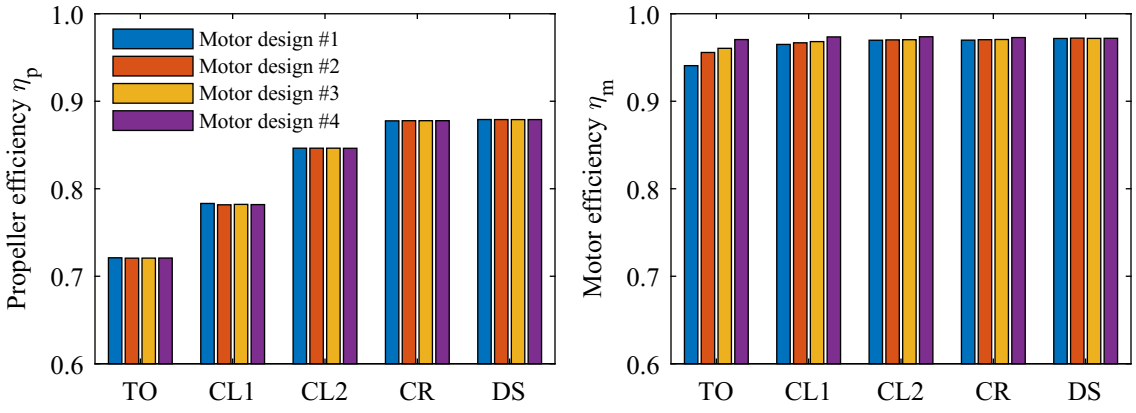

a) Propeller efficiency **b) Motor efficiency**

Fig. 9 Propeller and motor efficiencies for the different motor-propeller combinations; aerodynamic optimization.

To obtain further insight into the differences in motor efficiencies between the different motor-propeller combinations, the operating conditions of the propeller in the different mission segments were superimposed on the motor efficiency maps. Figure 10 presents the resulting maps for the different motors and all propeller designs, including the acoustic optimization results. The operating conditions at the different mission segments are indicated by the markers with labels. The order of the markers with respect to the mission was the same for all designs, with the torque requirement decreasing from take-off to descent. The results show that the performance benefit of increasing motor size is a direct

result of the wider envelope of peak motor efficiency. Both the optimum torque and rotational speed requirement from the propeller vary significantly during the mission. Therefore, the larger motor design, with a wider operating envelope, offers better-integrated energy efficiency over the entire mission.

Comparing the results for the different optimization objectives (indicated by the different levels of accepted energy penalty δE), Fig. 9 shows that acoustic optimization of the propeller drives the motor-propeller design towards lower rotational speed and thus higher torque values. This further stretches the operating domain of the motor-propeller combination, thereby limiting the performance of the smaller motor designs. The trend of decreasing rotational speed with increasing weight on the acoustic optimization is because the propeller noise emissions scale rapidly with the blade tip Mach number. For a given freestream condition, this tip Mach number can only be reduced by reducing rotational speed (i.e. increasing advance ratio). However, this comes at the cost of increased induced losses, which explains the performance penalty incurred by the acoustic optima shown in Fig. 8 [25].

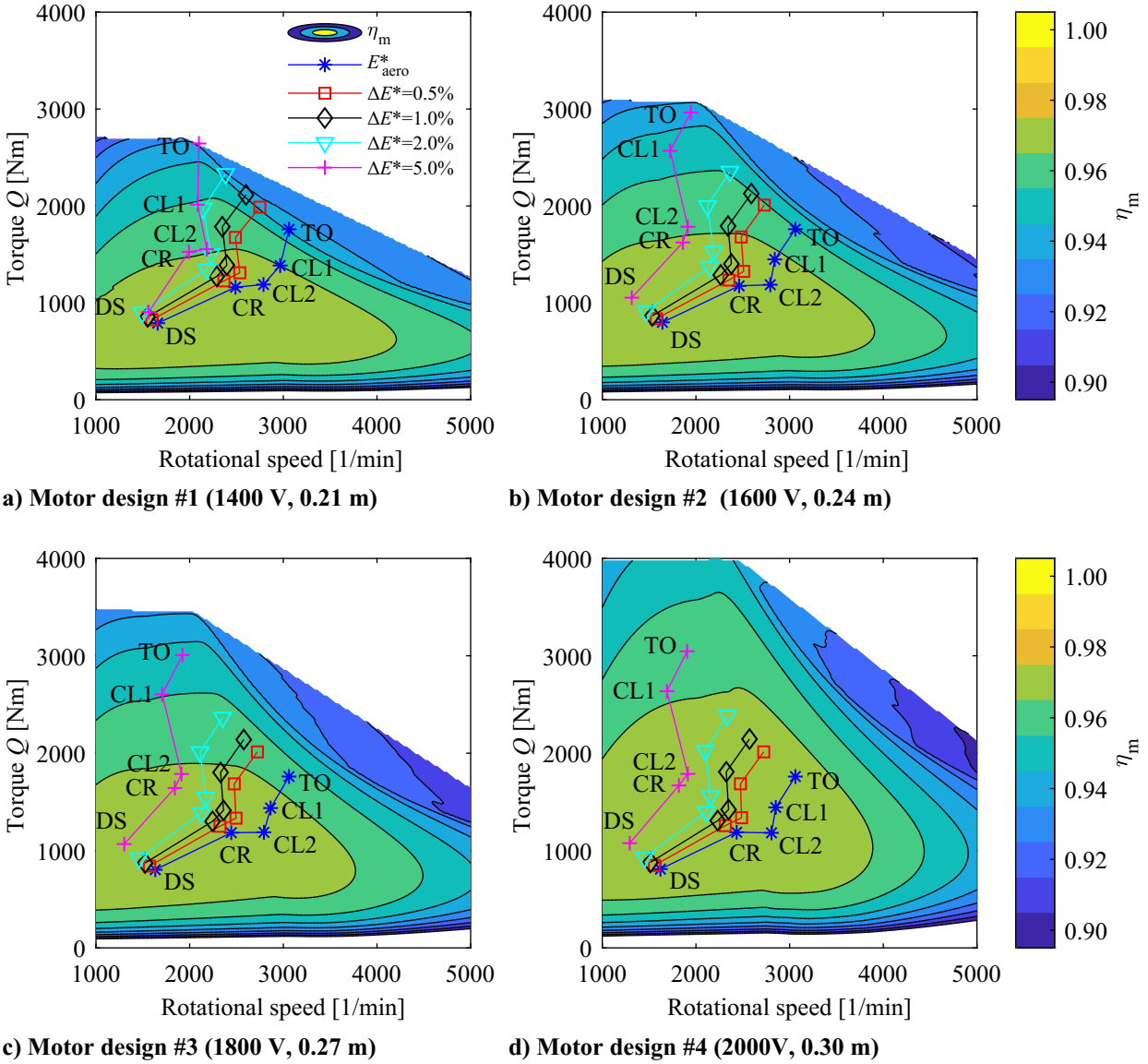

a) Motor design #1 (1400 V, 0.21 m) **b) Motor design #2 (1600 V, 0.24 m)**

c) Motor design #3 (1800 V, 0.27 m) **d) Motor design #4 (2000V, 0.30 m)**

Fig. 10 Motor efficiency maps with propeller operational points for each mission segment superimposed. E^*_{aero} indicates the aerodynamic optimum, ΔE^* the accepted energy penalty w.r.t the aerodynamic optimum in the acoustic optimizations.

Despite the significant change in performance between the motor-propeller combinations for the different motor

designs, the blade planform geometry of all propellers was very similar for a given objective function. Figure 11provides the radial distributions of chord and twist and a top view of the untwisted blade planforms. Results are compared between motor designs #1 and #4, both for the aerodynamic optima and the acoustic optima with a 2% energy penalty level.

It can be seen that for a given objective function, the propeller designs obtained for the different motor designs were very similar. For the aerodynamic optimization, the blade chord was equal to the predefined lower bound along the entire radius of the blade. The aerodynamic optimization favors slender blades to minimize induced losses, and for the given thrust requirements and the selected blade count, sufficient thrust could be produced with the minimum accepted blade chord. Similarly, the advance ratio was similar for all aerodynamic optima, because a low advance ratio is favored for high propeller efficiency, again to reduce induced losses. Therefore, the twist distributions were also similar for all motor-propeller combinations. As a result, for this objective, the performance difference between the different motor-propeller combinations was dominated by the differences in the motor efficiency maps.

For the acoustic objective, the advance ratio was increased to reduce the tip Mach number of the propeller, as discussed before. This requires an increase in the blade chord to satisfy the thrust requirement when compared to the aerodynamic optima. For this case, the wider operating envelope of motor design #4 enables operation at a 2-3% higher advance ratio in each mission segment compared to the motor-propeller combination with motor design #1, without energy-efficiency penalty. Therefore, the blade chord for the design with motor #4 is larger than for the design with motor #1. However, the differences are small, with an increase in chord of at most 3% around the outboard part of the blade ($r/R = 0.7$). Because of the small change in advance ratio, the twist distributions for both designs are very similar. Therefore, also for the acoustic optimization, the propeller efficiencies in each mission segment are again similar for the different motor-propeller combinations, and the motor efficiency dominates the changes in energy efficiency.

On an aircraft level, the decision to go with the motor design #4 would result in a heavier propulsion system than the motor design #1, due to the increased size of the motor, propeller characteristics, and the power train. As in the case of motor design #1, the lower voltage would impact the weight of the power train components such as DC bus distribution, cables, etc. For example, motor design #1 has a lower motor mass than motor design #4 but would have a higher cable mass in the power train, this would affect the overall performance of the aircraft. Due to the smaller efficiency envelope of motor design #1, the high-thrust demanding sections of the mission profile are operated in regions of lower efficiency and this would cause the motor to heat up faster. Also, motor design #1 cannot be operated for an extended period of time at these high-thrust demand points. Furthermore, this would increase the burden on the Thermal Management System (TMS), the TMS would have to be sized appropriately causing a weight penalty on the aircraft. The smaller motor, motor design #1, provides a lower maximum continuous thrust when compared to motor design #4 owing to the smaller drive voltage and length, as shown in Table 5. For safety considerations that are prevalent in the aerospace industry, motor design #1 may not be the best motor as the design

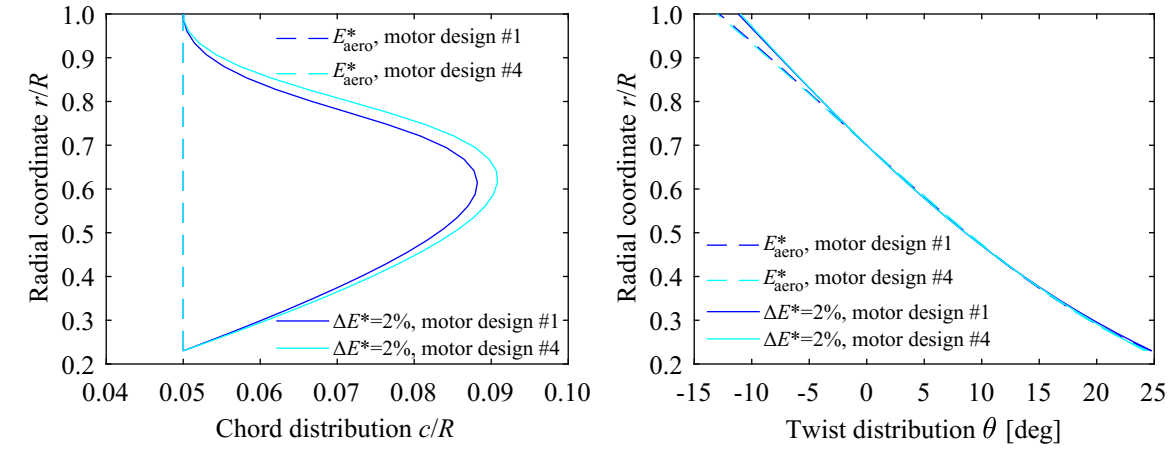

a) Chord distribution **b) Twist distribution**

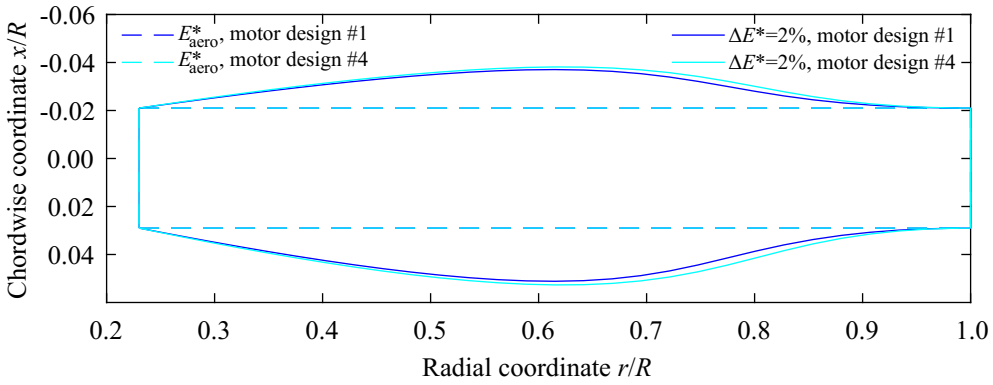

c) Top view of untwisted planforms

Fig. 11 Impact of optimization objective and motor design on propeller blade planform geometries.

VII. Conclusion

In this study, a coupled design methodology is explored and illustrated using the example of a motor and propeller integration. The study described in this paper has explored various system design parameters to match the propeller and electric machine from a holistic systems perspective. Aerodynamic and acoustic propeller performance have been evaluated and optimized in sequential with electric machine performance.

The integration of the propeller and the electric machine has been explored as an iterative collaborative process between the two disciplines. A larger motor design that provides a bigger peak efficiency envelope in the torque-rpm map provides better integrated energy efficiency over the entire mission. For smaller machines to achieve lower noise and higher energy efficiency, the machine's cooling needs to be considered especially for high demand flight phases To achieve this motor design parameters need to be studied in detail. For example, thermal analysis and a more detailed study on motor torque, while maintaining lower power density needs to be explored.

For a more comprehensive comparison of the integrated system and the aircraft-level impact of these decisions. A detailed model of the power train would be needed to understand the effect of the choice of propeller and motor on the power train and the aircraft. These integration studies were performed for a fixed mission, the impact of the integration on the off-design performance of the aircraft will have to be studied. Furthermore, when the design methodology is re-iterated with a revised mass and thrust requirement, a weighted metric such as energy consumed per passenger would have to be explored to capture which noise-efficiency trade-off is more beneficial to the aircraft.

Next steps and considerations for a holistic evaluation of the propeller-motor coupled designs:

- The implementation of each pair of coupled motor-propeller designs will have an impact on the aircraft, mission, and the rest of the powertrain design consequently the designs should be assessed holistically. In the present context, the propeller-coupled designs were optimized for the combined energy consumption of the motor and

propeller (energy provided to the motor). However, their evaluation cannot be isolated from the rest of the system and aircraft.

- Secondly, the rest of the powertrain (inverter, bus, converter, cables) should be re-designed so that it is compatible with the new motor voltage. The mass of each motor design, propeller, and rest of the electric powertrain components should be calculated to update the operating empty weight (OEW) of the aircraft. The aircraft platform is treated as a constraint and it is not re-redesigned, hence, the MTOW is a constraint.
- Consequently, the resulting operating empty weight for each motor-propeller coupled design will alter the payload capability of the aircraft. The payload capability can be translated into passenger capability.
- The next step would be to integrate the new component maps for the propeller, motor, and powertrain into the propulsion system calculations and re-iterate the flight mission analysis. The mission re-iteration of the new designs will result in new energy/fuel consumption and water emissions. The designs will be evaluated for the energy per passenger because it is a metric that captures the trade-off between the system mass, which is translated into passenger capability, and efficiency.
- To further expand the analysis and design evaluation, the coupled designs can be also tested in missions other than the design mission used in the propeller optimization of this paper. At the same time, the results of the aero-acoustic analysis should be assessed based on the noise certification standards for this class of aircraft and airport constraints so that the designs that may exceed the airport constraints can be rejected.

The objective of the iterative coupled design is that it refines the motor and propeller coupled design with the given constraint in their individual designs. More extensive design exploration will be carried out to capture design constraints for both components in future studies.

Acknowledgments

This project has received funding from the European Union's Horizon 2020 Research and Innovation Program under Grant Agreement No 875551. We also acknowledge the support we received from the ANSYS Motor-CAD support team and Dr. Bo Ren.

References

[1] McDonald, R. A., "Electric propulsion modeling for conceptual aircraft design," American Institute of Aeronautics and Astronautics Inc., 2014. https://doi.org/10.2514/6.2014-0536.

[2] McDonald, R. A., "Modeling of electric motor driven propellers for conceptual aircraft design," American Institute of Aeronautics and Astronautics Inc, AIAA, 2015. https://doi.org/10.2514/6.2015-1676.

[3] Lee, H. T., "A Technique for Matching Propeller, Motor, and Airframe of an Electric Powered Aircraft Based on Efficiency Maps," American Institute of Aeronautics and Astronautics Inc, AIAA, 2022. https://doi.org/10.2514/6.2022-0885.

[4] "Electric motor modeling for conceptual aircraft design," American Institute of Aeronautics and Astronautics Inc., 2013. https://doi.org/10.2514/6.2013-941.

[5] Bartlett, B. K., "Simulation of Configurable Hybrid Aircraft," Ph.D. thesis, California Polytechnic State Univeristy, San Luis Obispo, 2021.

[6] Kiran, A., Zaghari, B., Kipouros, T., and Reis, R. J. N. D., "Unpublished - Application of Model-Based Systems Engineering for the Integration of Electric Engines in Electrified Aircraft," IOP Publishing, 2023.

[7] Balachandran, T., Reband, J., Lewis, M., and Haran, K. S., "Co-Design of Integrated Propeller and Inner Rotor PMSM for Electric Aircraft Application," *2021 IEEE International Electric Machines Drives Conference (IEMDC)*, 2021, pp. 1–8. https://doi.org/10.1109/IEMDC47953.2021.9449579.

[8] Chandel, D., Reband, J. D., Hall, D. K., Balachandran, T., Xiao, J., Haran, K. S., and Greitzer, E. M., "Fan and Motor Co-optimization for a Distributed Electric Aircraft Propulsion System," *IEEE Transactions on Transportation Electrification*, 2022, pp. 1–1. https://doi.org/10.1109/TTE.2022.3204202.

[9] Hendershot, J., and Miller, T., *Design of Brushless Permanent-magnet Machines*, Motor Design Books, 2010. URL https://books.google.co.uk/books?id=n833QwAACAAJ.

[10] Vaez-Zadeh, S., *Control of Permanent Magnet Synchronous Motors*, Oxford University Press, 2018. https://doi.org/10.1093/oso/9780198742968.001.0001, URL https://doi.org/10.1093/oso/9780198742968.001.0001.

[11] Xie, P., Ramanathan, R., Vakil, G., and Gerada, C., "Simplified Analytical Machine Sizing for Surface Mounted Permanent Magnet Machines," *2019 IEEE International Electric Machines Drives Conference (IEMDC)*, 2019, pp. 751–757. https://doi.org/10.1109/IEMDC.2019.8785167.

[12] Yi, X., Yoon, A., and Haran, K. S., "Multi-physics optimization for high-frequency air-core permanent-magnet motor of aircraft application," Institute of Electrical and Electronics Engineers Inc., 2017. https://doi.org/10.1109/IEMDC.2017.8002293.

[13] Sirimanna, S., Thanatheepan, B., Lee, D., Agrawal, S., Yu, Y., Wang, Y., Anderson, A., Banerjee, A., and Haran, K., "Comparison of electrified aircraft propulsion drive systems with different electric motor topologies," *Journal of Propulsion and Power*, Vol. 37, 2021, pp. 733–747. https://doi.org/10.2514/1.B38195.

[14] Ibrahim, K., Sampath, S., and Nalianda, D., "Optimal Voltage and Current Selection for Turboelectric Aircraft Propulsion Networks," *IEEE Transactions on Transportation Electrification*, Vol. 6, 2020, pp. 1625–1637. https://doi.org/10.1109/TTE.2020.3004308.

[15] ATR, "ATR-72-600 Factsheet," , 2022. URL https://www.atr-aircraft.com/wp-content/uploads/2020/07/Factsheets_-_ATR_72-600.pdf.

[16] Laskaridis, P., and Pilidis, P., ""An Integrated Engine-Aircraft Performance Platform for Assessing New Technologies in Aeronautics"," Ph.D. thesis, Cranfield University, Cranfield UK, 2005.

[17] Sanders, D. S., and Laskaridis, P., "Full-Aircraft Energy-Based Force Decomposition Applied to Boundary-Layer Ingestion," *AIAA Journal*, Vol. 58, No. 10, 2020, pp. 4357–4373. https://doi.org/10.2514/1.J058695, URL https://doi.org/10.2514/1.J058695.

[18] Kirner, R., Raffaelli, L., Rolt, A., Laskaridis, P., Doulgeris, G., and Singh, R., "An assessment of distributed propulsion: Advanced propulsion system architectures for conventional aircraft configurations," *Aerospace Science and Technology*, Vol. 46, 2015, pp. 42–50. https://doi.org/https://doi.org/10.1016/j.ast.2015.06.022, URL https://www.sciencedirect.com/science/article/pii/S1270963815001996.

[19] Zhou, T., Enalou, H. B., Pontika, E., Zaghari, B., and Laskaridis, P., "Minimising the effect of degradation of fuel cell stacks on an integrated propulsion architecture for an electrified aircraft," *2022 IEEE Transportation Electrification Conference Expo (ITEC)*, 2022, pp. 1064–1069. https://doi.org/10.1109/ITEC53557.2022.9813899.

[20] Zhou, T., Enalou, H. B., Pontika, E., Zaghari, B., Kipouros, T., and Laskaridis, P., "The Impact of Multi-Stack Fuel Cell Configurations on Electrical Architecture for a Zero Emission Regional Aircraft," American Institute of Aeronautics and Astronautics Inc., 2023.

[21] Zaghari, B., Zhou, T., Balaghi, H. E., Pontika, E., Kipouros, T., and Laskaridis, P., "The Impact of Multi Stack Fuel Cell Configurations on Electrical Architecture for a Zero Emission Regional Aircraft," *AIAA SciTech*, 2023.

[22] Zhou, T., Enalou, H. B., Pontika, E., Zaghari, B., and Laskaridis, P., "Minimising the effect of degradation of fuel cell stacks on an integrated propulsion architecture for an electrified aircraft," *2022 IEEE Transportation Electrification Conference & Expo (ITEC)*, IEEE, 2022, pp. 1064–1069.

[23] Li, Q., Öztürk, K., Sinnige, T., Ragni, D., Wang, Y., Eitelberg, G., and Veldhuis, L. L. M., "Design and Experimental Validation of Swirl Recovery Vanes for Propeller Propulsion Systems," *AIAA Journal*, Vol. 56, No. 12, 2018, pp. 4719–4729. https://doi.org/10.2514/1.J057113.

[24] Stokkermans, T. C. A., and Veldhuis, L. L. M., "Propeller Performance at Large Angle of Attack Applicable to Compound Helicopters," *AIAA Journal*, Vol. 59, No. 6, 2021, pp. 2183–2199. https://doi.org/10.2514/1.J059509.

[25] Sinnige, T., de Gruijl, W., de Haan, W., and Eitelberg, G., "Rapid Aeroacoustic Planform Design Optimization of Installed Propellers," *33rd Congress of the International Council of the Aeronautical Sciences*, ICAS Paper 2022-0489, Sept. 2022.

[26] Yu, Z., Li, Y., Jing, Y., and Wang, J., "Cooling System of Outer Rotor SPMSM for a Two-Seater All-Electric Aircraft Based on Heat Pipe Technology," *IEEE Transactions on Transportation Electrification*, Vol. 8, No. 2, 2022, pp. 1656–1664. https://doi.org/10.1109/TTE.2021.3127555.

[27] Popescu, M., Staton, D., Boglietti, A., Cavagnino, A., Hawkins, D., and Goss, J., "Modern heat extraction systems for electrical machines - A review," *2015 IEEE Workshop on Electrical Machines Design, Control and Diagnosis (WEMDCD)*, 2015, pp. 289–296. https://doi.org/10.1109/WEMDCD.2015.7194542.

https://dspace.org/

The impact of electric machine and propeller coupling design on electrified aircraft noise and performance

Zaghari, Bahareh; Kiran, Abhishek; Sinnige, Tomas; Pontika, Evangelia; Enalou, Hossein B. ...

2023-01-19
American Institute of Aeronautics and Astronautics (AIAA)
https://doi.org/10.2514/6.2023-2133
Zaghari B, Kiran A, Sinnige T, et al., (2023) The impact of electric machine and propeller coupling design on electrified aircraft noise and performance. In: AIAA SciTech Forum 2023, 23-27 January 2023, National Harbor, Maryland, USA. Paper number AIAA 2023-2133

Downloaded from a DSpace repository. https://dspace.org/